

## Article

# Frontal Vehicular Crash Energy Management Using Analytical Model in Multiple Conditions

Danqi Wang<sup>1,2</sup>, Junyuan Zhang<sup>3</sup>, Shihang Wang<sup>3</sup> and Lin Hu<sup>1,\*</sup> 

<sup>1</sup> College of Automotive and Mechanical Engineering, Changsha University of Science & Technology, Changsha 410000, China

<sup>2</sup> State Key Laboratory of Automobile Safety and Energy Conservation, Tsinghua University, Beijing 100000, China

<sup>3</sup> State Key Laboratory of Automobile Simulation and Control, Jilin University, Changchun 130015, China

\* Correspondence: hulin@csust.edu.cn

**Abstract:** When it comes to frontal vehicular crash development, matching the stiffness of the front-end structures reasonably, i.e., impact energy management, can effectively improve the safety of the vehicle. A multi-condition analytical model for a frontal vehicular crash is constructed by a three-dimensional decomposition theory. In the analytical model, the spring is used to express the equivalent stiffness of the local energy absorption space at the front-end structure. Then based on the analytical model, the dynamic responses and evaluation indexes of the vehicle in MPDB and SOB conditions are derived with the input of the crash pulse decomposition scheme. Comparing the actual vehicle crash data and the calculation results of the proposed solution method, the error is less than 15%, which verifies validity of the modeling and the accuracy of the solution. Finally, based on the solution method in the MPDB and the SOB conditions, the sensitivities of the crash pulse decomposition scheme to evaluation indexes are analyzed to obtain qualitative rules which guide crash energy management. This research reveals the energy absorption principle of the front-end structure during the frontal impact process, and provides an effective optimization method to manage the multiple conditions of the vehicle crash energy such as the FRB (frontal rigid barrier), the MPDB (mobile progressive deformable barrier), and the SOB (small overlap barrier).

**Keywords:** crash energy management; front-end structure; modelling; multiple conditions; vehicle



**Citation:** Wang, D.; Zhang, J.; Wang, S.; Hu, L. Frontal Vehicular Crash Energy Management Using Analytical Model in Multiple Conditions. *Sustainability* **2022**, *14*, 16913. <https://doi.org/10.3390/su142416913>

Academic Editor: Marilisa Botte

Received: 18 November 2022

Accepted: 12 December 2022

Published: 16 December 2022

**Publisher's Note:** MDPI stays neutral with regard to jurisdictional claims in published maps and institutional affiliations.



**Copyright:** © 2022 by the authors. Licensee MDPI, Basel, Switzerland. This article is an open access article distributed under the terms and conditions of the Creative Commons Attribution (CC BY) license (<https://creativecommons.org/licenses/by/4.0/>).

## 1. Introduction

The process of an automobile crash includes the following three parts: barriers, vehicles, and occupants, and is a complex dynamics system. According to the annual statistical report of road traffic accidents from the Chinese government, frontal impact of automobile accidents account for the highest proportion among all accident forms [1,2]. In a frontal crash, the crash energy is absorbed by the front-end structures of vehicle [3]. With the development of crash safety regulations, today's vehicle front-end structural design needs to meet the requirements of multiple conditions such as FRB (frontal rigid barrier), MPDB (mobile progressive deformable barrier), and SOB (small overlap barrier) [4,5]. This greatly increases the difficulty of the vehicle safety design. From the perspective of dynamics, revealing the crash energy dissipation mechanism and constructing a dynamic model of the front-end structure, which solves energy management in the early design stage, is of great significance for improving the safety of the vehicle [6].

The ultimate goal of vehicular frontal crash safety research is to protect the safety of its occupants. In the crash process, the initial kinetic energy of the occupants is dissipated through the following two ways: the deformation of the vehicle structure and the action of the restraint system [7]. According to statistics about existing vehicles, the structure absorbs more than 60% of the kinetic energy of the occupants and is the most important way to absorb energy [8,9]. Crash energy management is meant to control the dissipation of energy

by designing the rigidity and deformation of the vehicle structure so as to protect the safety of the occupants. In the process of a vehicular frontal crash, the energy dissipation is related to the topology of the auto body and the transmission path of the impact force [10,11].

During the process of a frontal vehicular crash, the total energy of the system is mainly absorbed through the deformation of the front-end structures. In theory, the product of force and displacement is equal to energy. Thus the crash energy absorbed by the vehicle is approximately equal to the product of the impact force and the deformation of the front-end structures [8]. The mass loss of the vehicle in a frontal crash is negligible compared with the total weight. In other words, the mass of the vehicle during the collision is approximately constant. In theory the impact force is approximately equal to the product of the acceleration and mass. Similar conclusions were also demonstrated in reference [12], which defines crash energy per unit mass as energy density. Then, the energy density absorbed by the vehicle during the impact is the product of the acceleration and the structural deformation [8,13]. When the vehicle hits FRB, almost all of the crash energy is absorbed by the structural deformation. In this process, the vehicle acceleration is also called the crash pulse. The sum of the deformations of all vehicle structures in the longitudinal direction (the driving direction) is the maximum dynamic crushing. The maximum dynamic crushing is obtained by the quadratic integration of the crash pulse [12,14]. That is to say, the crash energy is integral to the crash pulse in the displacement domain. Therefore, from the perspective of mechanics, the frontal crash energy management of the vehicle is actually the design and the decomposition problems of the crash pulse [8].

The design problem of the crash pulse has been extensively studied through theories, simulations, and experiments [15–17]. At present, there are relatively mature methods and qualitative conclusions for guiding engineering design of crash pulses [18,19]. In terms of engineering conclusions, without considering the engine layout, the high-low-height crash pulse can effectively reduce occupant injuries; the double-step crash pulse is suitable for vehicles considering the engine layout, and the higher first step, the lower second step are the better for occupant safety [7]. As a continuation of the paper on multi-condition optimization of crash pulse, this article focuses on the decomposition of the crash pulse.

In this paper, the crash pulse in the displacement domain is the total energy target during the impact process which is then decomposed into absorption energies of sub-structures based on the topology and the load path of vehicle. To achieve this, it is necessary to find the correlation between the target crash pulse and the structural performance. From 2006 to 2011, the magic cube approach was proposed to decompose the crash energy into sub-structure design goals from the three-dimensions of time, space, and size, and design the load of the front longitudinal beams through the dynamic topology optimization method [20,21]. In 2011, the energy-absorbing space of the front-end structure is divided into four layers in the vertical direction according to the transmission path of impact force, and used to derive the design goals of energy absorption by the simplified model [22]. In 2016, the vehicle longitudinal energy management method and the lateral energy management method are summarized to divide the front-end structure longitudinally, and then decompose the energies of each area according to the horizontal arrangement of the energy absorbing structure [7,23].

Our team has studied the frontal vehicular crash mechanics, crash pulse optimization, and energy management methods in the early stage. In the reference [12], we analyzed the energy dissipation process of a frontal vehicular crash and established the relationship between crash pulse and energy from the perspective of mechanics. In the references [15,24], we discussed the coupling relationship between the crash pulse and auto body structures, and established an automatic optimization method for the crash pulse considering multiple impact conditions. In the references [13,25,26], the energy absorption space of front-end structures is vertically layered and longitudinally segmented by the deformation mode of the sub-structures to obtain the decomposing energy as the design targets of anti-collision beam, the energy absorbing box, and the longitudinal beam.

At present, it is mainly focused on the research of crash energy management methods of the vehicle front-end structure based on engineering experience in the FRB impact condition [27–29]. Considering the impact force transmission characteristics of FRB condition, the front-end structure of the vehicle is divided into space, and the crash pulse is decomposed according to the sub-space as the energy absorption target [12]. In addition to FRB condition, the vehicle also needs to absorb energy through the deformation of the front-end structure in other frontal impact conditions, such as the MPDB impact condition which mainly test crash compatibility and SOB impact conditions which mainly test the safety of the passenger compartment [5,30,31]. Therefore, managing the energy absorption of front-end structures to meet the performance requirements and evaluation indicators of multiple frontal crash conditions is an urgent problem in the vehicle design industry, and it is also the research purpose of this paper.

Based on the frontal multi-condition crash pulse design method studied in the previous stage, this paper proposes a multi-condition crash energy management method, that is, the decomposition method of crash pulse. The proposed method optimizes the energy absorption of the vehicle front-end structures considering the design requirements of three conditions (that is FRB, MPDB, and SOB). The method can help enterprises to carry out the forward design of frontal vehicular crashes when the empirical data are insufficient. The main contributions of this paper include the following three aspects: (1) constructing a three-dimensional analytical model of vehicle front-end structure to describe the energy absorption space, impact load path, and structural stiffness; (2) deriving the dynamic responses and evaluation indexes of vehicle and barrier in the MPDB and SOB conditions to realize the crash pulse decomposition considering multiple conditions based on the proposed analytical model; (3) analyze the sensitivity of the crash pulse decomposition scheme to the evaluation indexes to obtain the qualitative crash pulse energy management strategy based on the analytical model.

The paper is organized as follows: Section 2 introduces a mechanical analytical model of vehicle front-end structure. In Section 3, we derive the solution of analytical model in MPDB and SOB conditions. An empirical case and the simulation results of existing vehicles that have been running in China are applied to verify this constructed model and the solution method in Section 3. Analysis and discussion are conducted in Section 4. Finally, the conclusions of this paper are drawn in Section 5.

## 2. Three-Dimensional Analytical Model of Vehicle Front-End Structure

### 2.1. Three-Dimensional Decomposition of Energy Absorption Space

In this section, the energy absorption space during a frontal impact can be determined as shown in Figure 1, where  $B$  represents the width of the whole vehicle;  $H$  represents the vertical distance from the intersection point of pillar  $A$  and the front finger beam to the chassis;  $D$  represents the longitudinal space  $L$  in the forward compartment of the vehicle minus the engine or motor occupancy  $E$ . The total energy absorption space can be decomposed into longitudinal, lateral, and vertical dimensions as follows, also considering the overlap rate of impact conditions, topological structure of the car body, and the layout position of the engine and motor.

**Lateral decomposition:** On both sides of the body symmetry plane, the energy absorption structure of the vehicle is almost exactly the same, and the contact area between the vehicle and the wall barrier in MPDB impact condition is also 50% of the width of the vehicle. Thus, the total energy absorption space can be divided horizontally into two equal regions. To ensure a better safety level of the vehicle in the condition of 25% small bias impact, the energy absorption structure should be set within 25% wide range on both sides of the vehicle. If the requirements of meeting various impact conditions are considered at the same time, four regions can be divided horizontally. The width of each region is 25% of the total car width.

**Longitudinal decomposition:** According to the impact force transfer path of the vehicle in the frontal impact, the total energy absorption space can be vertically divided into two,

three, and four tiers longitudinally. Take a typical passenger vehicle as an example, which includes four tiers of the total energy-absorbing space, the first tier is the engine cover; the second one is the front finger beam; the third one is the anti-impact beam, energy absorption box, and longitudinal beam; and the fourth one is the sub-frame structure. The energy absorption corresponds to the impact force. The energy absorption of each tier accounts for about 10%, 20%, 50%, and 20% of the total energy absorption, respectively [22]. The third tier includes the main energy absorption area of the vehicle. To improve the lightweight effect of vehicles, the engine hood is designed to be thinner and absorb less energy, so the energy absorption space is mainly divided into three tiers, that is, the first tier contains the engine hood, front finger beam and other structures. In addition, the sub-frames of some vehicles are removed in consideration of the economic and lightweight factors, so that the longitudinal space is two tiers.

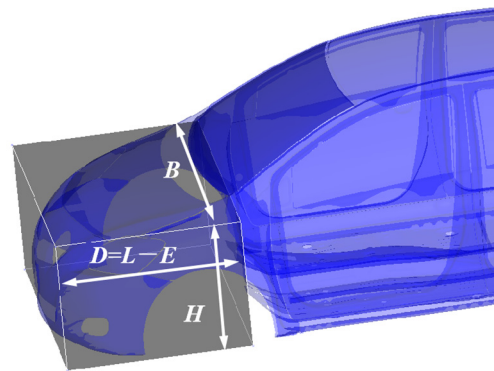


**Figure 1.** The energy absorption space during a frontal impact.

**Vertical decomposition:** The engine of the traditional automobile and the motor of a pure electric vehicle almost do not deform during the impact, which can be regarded as a rigid structure; therefore, according to the layout position of rigid components such as engine or motor, the total space of energy absorption can be divided longitudinally. For traditional gasoline cars and hybrid cars, rigid components such as engine need to be placed in the middle of the front end firewall considering the connection between the engine and drive shaft and maintenance problems. Thus, the two sections from the front end of the engine to the anti-impact beam and from the back end of the engine to the firewall are set as impact energy absorption spaces. For pure electric vehicles, the motor can be considered close to the firewall layout because there is no drive shaft on the vehicle. In this way, the hole from the anti-impact beam to the front end of the motor can be used as a section of energy absorption space.

In general, the three-dimensional decomposition of the total space of energy absorption at the front end of vehicle is to take into account the impact condition, the transmission path of impact force, and the arrangement of the engine and motor, etc., and conduct horizontal division, vertical stratification, and longitudinal segmentation successively. The decomposed fore cabin energy absorption space becomes the accumulation of the energy absorption subspace. As a sample, the total space of energy absorption at the front end of vehicle is decomposed  $4 \times 3 \times 2$  sections as shown in Figure 2.

## 2.2. Three-Dimensional Decomposition of Crash Pulse

In the FRB impact condition, the wall is rigid and the overlap rate between the vehicle and the wall is 100%. This indicates that almost all the energy absorption structures in the front end of the vehicle are involved in deformation energy absorption during the impact, and the acceleration response of the vehicle, namely the crash pulse, is also the result of the comprehensive action of the energy absorption structure. Thus, we take the crash pulse of FRB condition as the overall energy absorption objective of the vehicle's front end structure, and gradually decompose it into each energy absorption subspace and the design target

of the energy absorption structure in space, so as to achieve the forward design of the front-end structure.

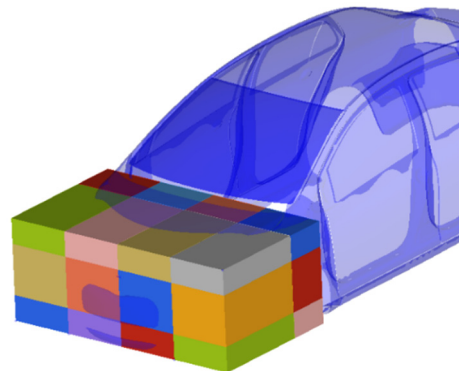


**Figure 2.** Three-dimensional decomposition of the total energy absorption space of automobile front compartment.

The horizontal coordinate of the crash pulse in the displacement domain is the deformation, which corresponds to the longitudinal direction of the energy absorption space, but there is no difference between the lateral direction and the vertical direction. Therefore, the three-dimensional decomposition method proposed in this section is mainly to decompose the crash pulse into each energy-absorbing subspace in accordance with a given proportion according to the three-dimensional decomposition scheme of the total energy-absorbing space. If the longitudinal part of the total energy absorbing space is divided into two parts, the crash pulse is divided into two parts at the deformation corresponding to the longitudinal subspace.

When the front energy absorption space of the vehicle is divided into  $N$  tiers vertically and  $M$  zones horizontally, the decomposition scheme  $Q$  of the crash pulse is obtained as shown in Figure 3. Note that the percentage of the absorbed energy of the sub-absorbent space in the total absorbed energy is represented by  $q_{nm}$  ( $n = 1, 2, \dots, N; m = 1, 2, \dots, M$ ).

$$Q = \begin{bmatrix} q_{11} & q_{12} & \cdots & q_{1M} \\ q_{21} & q_{22} & \cdots & q_{2M} \\ \vdots & \vdots & \ddots & \vdots \\ q_{N1} & q_{N2} & \cdots & q_{NM} \end{bmatrix} \tag{1}$$

$$\begin{cases} Q_{Ym} = q_{1m} + q_{2m} + \dots + q_{Nm}, m = 1, 2, \dots, M \\ Q_{nZ} = q_{n1} + q_{n2} + \dots + q_{nM}, n = 1, 2, \dots, N \end{cases} \tag{2}$$

$q_{11}$	$q_{12}$	$\cdots$	$q_{1m}$	$Q_{Z1}$
$q_{21}$	$q_{22}$	$\cdots$	$q_{2m}$	$Q_{Z2}$
$\vdots$	$\vdots$	$\ddots$	$\vdots$	$\vdots$
$q_{n1}$	$q_{n2}$	$\cdots$	$q_{nm}$	$Q_{Zn}$
$Q_{Y1}$	$Q_{Y2}$	$\cdots$	$Q_{Ym}$	

**Figure 3.** Preliminary decomposition scheme of frontal impact energy.

In Equations (1) and (2),  $Q$  represents the total absorbed energy;  $Q_{Ym}$  represents the absorbed energy of  $m$ th region,  $m = 1, 2, \dots, M$ ;  $Q_{Yn}$  represents the absorbed energy of  $n$ th tier,  $n = 1, 2, \dots, N$ .

### 2.3. Construction of Analytical Model

After the three-dimensional decomposition of the total energy absorption space, each subspace corresponds to a decomposed crash pulse, or a sub-pulse. It is the same as the original pulse in shape, but the amplitude is different, which is the product of the original pulse and the proportion of energy absorbed by each subspace. The crash pulse in the displacement domain can be regarded as the equivalent specific stiffness of the front-end structure of the vehicle; similarly, the sub-pulse decomposed to each energy-absorbing subspace can be regarded as the equivalent specific stiffness of the space.

Figure 4 represents the three-dimensional vehicle analytical model for frontal impact. In this model, the equivalent specific stiffness of each energy-absorbing subspace is expressed by spring stiffness  $k_{ij}$ , rigid bodies such as engine, motor, and passenger cabin are expressed by a mass block.

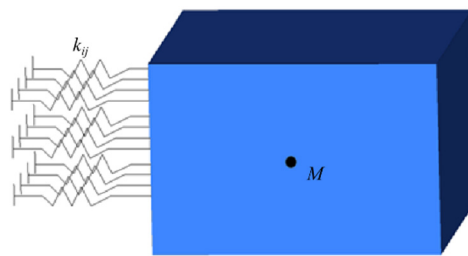


Figure 4. Three-dimensional vehicle analytical model.

The spring stiffness  $k_{ij}$  can be calculated as follows:

$$k_{ij} = q_{ij} \cdot \frac{a_v}{d_v} \cdot M \tag{3}$$

where,  $a_v$  represents the crash pulse;  $d_v$  represents vehicle displacement;  $M$  represents vehicle mass;  $i$  is the number of lateral decomposition of the total space of energy absorption in the front compartment, and  $j$  is the number of vertical decomposition of the total space of energy absorption.

### 3. Solution of Analytical Model in Multi-Conditions of a Frontal Vehicular Crash

#### 3.1. Solution Method for MPDB Condition

In the MPDB impact system, it mainly consists of the following two parts: barrier and vehicle. The impact process of the MPDB condition is defined as the process in which the vehicle and the barrier start to contact either of them with a deceleration of 0. It is assumed that the masses of the MPDB and vehicle are constant and the energy-absorbing structures of the two are only plastically deformed without elastic deformation during the impact process. Due to the rotations of vehicle and barrier are all small during the impact process, structural deformation is the most important way to absorb energy [24]. The simplified model of MPDB condition can be constructed ignoring the energy converted to rotation as shown in Figure 5.

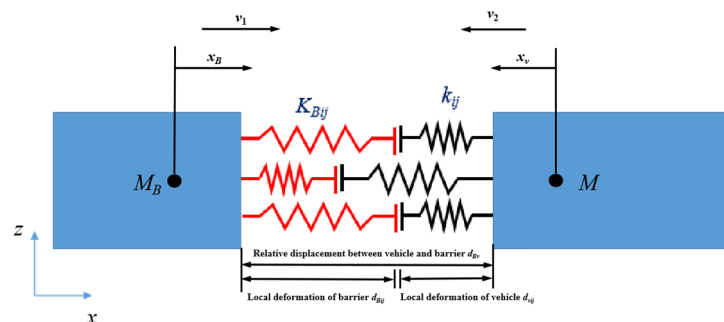


Figure 5. The simplified model of MPDB condition.

In this model, the barrier parameters obtained in the conceptual design stage include the mass and equivalent stiffness of the barrier, the general layout parameters of the vehicle, including the energy absorption space of the front-end structure and the mass of the vehicle as the system parameters. Taking the crash pulse of vehicle FRB condition as input; the dynamic response of the vehicle and the barrier during the impact was solved, and the vehicle compatibility evaluation indexes are calculated.

In Figure 5, the vehicle and the barrier move in relative motion;  $M$  and  $M_B$  are the masses of the vehicle and the barrier;  $d_{Bv}$  is their relative displacement;  $d_{ij}$  is the local deformation of the vehicle;  $d_{Bij}$  is the local deformation of the barrier;  $k_{ij}$  is the local stiffness of the vehicle, and  $k_{Bij}$  is the local stiffness of the barrier.

During the impact, the local stiffness of the vehicle and the barrier,  $k_{ij}$  and  $k_{Bij}$ , are first connected in series to obtain the equivalent stiffness  $k_{eqij}$  of each energy absorption subspace, and then the equivalent stiffness of each energy absorption subspace is connected in parallel to obtain the equivalent stiffness  $K_{eq}$  of the vehicle and the barrier, as follows:

$$\begin{cases} k_{eqij} = \frac{k_{Bij} \cdot k_{ij}}{k_{Bij} + k_{ij}} \\ K_{eq} = \sum k_{eqij} \end{cases} \quad (4)$$

$$\begin{cases} M_{eq} = \frac{M_B \cdot M}{M_B + M} \\ v_{eq} = \frac{v_0 \cdot v_0}{v_0 + v_0} = \frac{v_0}{2} \end{cases} \quad (5)$$

where,  $M_{eq}$  represents the equivalent mass of the model, and  $v_{eq}$  represents the equivalent velocity.

The motion response of the vehicle and the barrier is obtained as follows:

$$\begin{cases} d_B(t) = \frac{M}{M_B + M} \cdot \frac{2v_0}{\omega} \cdot \sin(\omega \cdot t) \\ d_v(t) = \frac{M_B}{M_B + M} \cdot \frac{2v_0}{\omega} \cdot \sin(\omega \cdot t) \end{cases} \quad (6)$$

$$\begin{cases} d_B(t) = \frac{M}{M_B + M} \cdot (-2 \cdot v_0 \cdot \omega \cdot \sin(\omega \cdot t)) \\ d_v(t) = \frac{M_B}{M_B + M} \cdot (-2 \cdot v_0 \cdot \omega \cdot \sin(\omega \cdot t)) \end{cases} \quad (7)$$

$$\begin{cases} v_B(t) = v_0 - \int a_B(t) dt \\ v_v(t) = v_0 - \int a(t) dt \end{cases} \quad (8)$$

$$\omega = \sqrt{\frac{K_{eq}}{M_{eq}}} \quad (9)$$

where,  $d_B$  and  $d_v$  are respectively for the barrier and the deformation of the vehicle impact process;  $a_B$  and  $a_v$  are respectively for the barrier and the vehicle acceleration,  $v_B$  and  $v_v$  are the barrier and the vehicle speed, respectively;  $\omega$  is the natural frequency of the impact system.

In addition, three compatibility evaluation indexes of MPDB condition, i.e., the relative motion displacement of the vehicle and the barrier ( $d_{Bv}$ ), the uniformity index of the barrier ( $SD$ ), and the maximum deformation of the barrier ( $MD$ ), as follows:

$$d_{Bv} = d_B + d_v \quad (10)$$

$$d_{Bij} = d_{Bv} \times \frac{k_{ij}}{k_{Bij} + k_{ij}} \quad (11)$$

$$SD = \sqrt{\frac{1}{m} \times \sum (d_{Bij} - \bar{d}_{Bij})^2} \quad (12)$$

$$d_{Bmax} = \max(d_{Bij}) \quad (13)$$

where,  $m$  represents the number of forward compartment subspaces that absorb energy.

### 3.2. Solution for Small Overlap Condition

In the small overlap condition, the vehicle decelerates along the longitudinal direction and rotates around its contact point with the rigid barrier after contacting with the barrier. If one of the following two point occurs, the impact process of small overlap condition is considered to be over: (1) when the speed of the vehicle decreases to 0, the structures of the vehicle no longer deform longitudinally; (2) if the vehicle displacement in the Y direction is  $\geq 25\%$  of the vehicle width, the vehicle is detached with the barrier without structural deformation. Therefore, the vehicle motion responses in the impact process of the small overlap condition can be considered from two aspects, i.e., the deceleration motion and rotation motion of the vehicle.

Based on the theory of impact mechanics, the simplified model of small overlap condition can be obtained as shown in Figure 6. In this model,  $O$  is the contact point between the vehicle and the barrier, and also the rotation center of the vehicle.  $v_0$  is the impact speed,  $M$  is the mass of the vehicle, and  $k_{ij}$  is the vehicle stiffness.

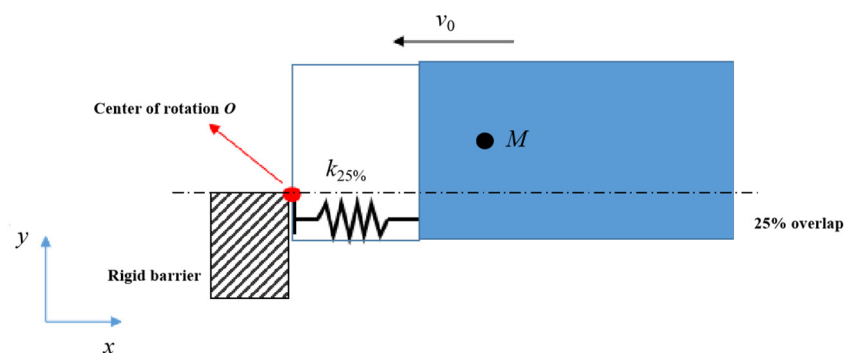


**Figure 6.** The simplified model of small overlap condition in longitudinal.

The motion response of the vehicle in this condition can be considered from two aspects, i.e., the deceleration motion and the rotation motion of the vehicle. The 25% overlap area between the vehicle and the barrier is mainly the energy-absorbing area during the impact, and its equivalent stiffness ( $k_{25\%}$ ) is calculated as follows:

$$k_{25\%} = \sum k_{i2} \quad (14)$$

The vehicle makes a single-degree-of-freedom free vibration in the X-axis direction. The vibration equation is as follows:

$$M\ddot{x}(t) + k_{25\%}x(t) = 0 \quad (15)$$

where,  $x(t)$  is the displacement of the vehicle, and  $\ddot{x}(t)$  is the acceleration response of the vehicle.

$$\omega = \sqrt{\frac{k_{25\%}}{M}} \quad (16)$$

$$\begin{cases} x(t) = A \sin(\omega t + \phi) \\ \dot{x}(t) = A\omega \cos(\omega t + \phi) \\ \ddot{x}(t) = -A\omega^2 \sin(\omega t + \phi) \end{cases} \quad (17)$$

In this condition,  $t = 0$ ,  $x = 0$ , and  $\dot{x} = v_0$ . Thus, the motion response of the vehicle is obtained as follows:

$$\begin{cases} x_v = x(t) = \frac{v_0}{\omega} \sin(\omega t) \\ v_v = \dot{x}(t) = v_0 \cos(\omega t) \\ a_v = \ddot{x}(t) = -v_0\omega \sin(\omega t) \end{cases} \quad (18)$$

The force analysis of the vehicle under the condition of the small overlap condition is shown in Figure 7. The vehicle will rotate around point  $O$  under the action of impact reaction  $F$ , and the distance between the vehicle's center of mass and the center of rotation

is the radius of rotation  $r$ . When the vehicle is decelerating, its longitudinal displacement is  $x_v$ , and the longitudinal distance between the center of mass and the center of rotation is  $1/2L - x_v$ . When the vehicle is rotating, the transverse displacement of the center of mass is  $y$ , and the transverse distance from the center of mass to the center of rotation is  $25\% B + y$ .

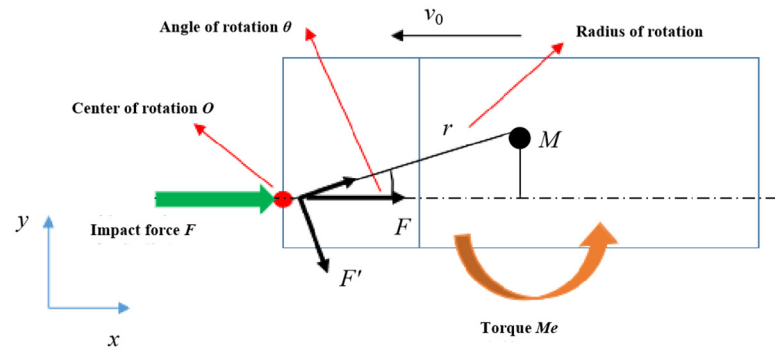


**Figure 7.** The simplified model of small overlap condition in rotation.

The radius of rotation ( $r$ ) and the rotation angle ( $\theta$ ) of the vehicle are calculated as follows:

$$r = \sqrt{(y + 0.25 \cdot B)^2 + (1/2 \cdot L - x_v)^2} \quad (19)$$

$$\theta = a \cdot \tan\left(\frac{y + 0.25 \cdot B}{1/2 \cdot L - x_v}\right) \quad (20)$$

The torque of the vehicle ( $Me$ ), the angular acceleration of the vehicle rotation ( $\beta$ ), and the lateral displacement of the vehicle ( $y$ ) is obtained as follows:

$$M_e = F' \cdot r = F \cdot \sin(\theta) \cdot r = F \cdot (y + 0.25 \cdot B) \quad (21)$$

$$M_e = F' \cdot r = J \cdot \beta \quad (22)$$

$$y = r \cdot \sin(\theta) - 0.25 \cdot B \quad (23)$$

where,  $F'$  represents the component force of the impact reaction  $F$  perpendicular to the direction of the radius of rotation;  $J$  represents the moment of inertia of the vehicle.

The maximum longitudinal displacement of the vehicle is the structural deformation of the vehicle in the process of impact. The intrusion of the crew compartment ( $D_{25\%max}$ ) can be calculated as follows:

$$D_{25\%max} = \max(x_v) - L_1 \quad (24)$$

### 3.3. Verification

#### 3.3.1. Evaluation Indexes

##### (1) Occupant load criterion (OLC)

The OLC is calculated by the velocity–time curve of the barrier as Figure 8. A smaller OLC is preferable [19]. At the time  $t_1$  in the Figure 8, the virtual occupant makes free movement relative to the barrier, and the displacement is  $S_1 = 0.065$  m; from the time  $t_1$  to  $t_2$ , the relative displacement between virtual occupant and barrier is  $S_2 = 0.235$  m.

##### (2) Maximum deformation (MD)

If there is an intrusion depth of 0.63 m in an area larger than  $40 \text{ mm} \times 40 \text{ mm}$  on the barrier, the barrier is considered to be bottoming out. At the time, deduction of two points is  $MD = 2$ , otherwise  $MD = 0$ .

##### (3) Standard deviation (SD)

The SD of barrier intrusion is obtained by the homogeneity of footprint based on scans of barrier. A smaller SD is preferable. The barrier deformation uniformity factor  $h$  is calculated by SD as follows:

$$\begin{cases} \text{if } SD < 50\text{mm}, & h = 0 \\ \text{if } 50\text{mm} < SD < 150\text{mm}, & h = (SD - 50)/100 \\ \text{if } SD > 150\text{mm}, & h = 1 \end{cases} \quad (25)$$

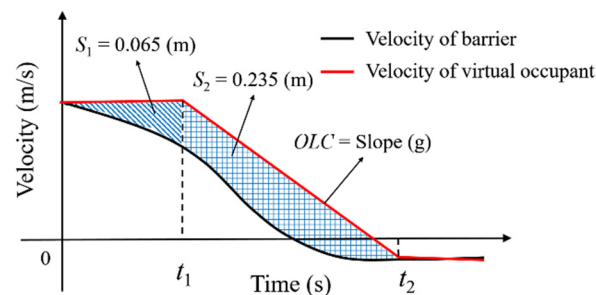


Figure 8. The OLC calculated by velocity–time curve of barrier.

(4) The penalty of Mcompat (PM)

The calculation rules for PM reference to [31] are shown in the following:

$$\begin{cases} \text{if } OLC < 25g, \\ \quad M_{compat} = -2 \cdot h - MBO; \\ \text{if } 25g \leq OLC \leq 40g, \\ \quad M_{compat} = -2 \cdot OLC/15 + 10/3 \\ \quad \quad - h \cdot ((4 \cdot OLC/10 - 8) - (2 \cdot OLC/15 - 10/3)) - MBO; \\ \text{if } OLC > 40g, \\ \quad M_{compat} = -2 - 6 \cdot h - MBO. \end{cases} \quad (26)$$

### 3.3.2. Verification of MPDB Condition

The main MATLAB algorithm of the solution method is established as shown in the Supplementary Information. The data about three quality grade vehicles in FRB and MPDB tests [30] are used to verify the accuracy and reliability of the solution method. In this condition, research of the influence of pulse parameters and vehicle quality on the evaluation index, including OLC, MD, SD, and PM, three kinds of vehicles, i.e.,  $V_1$ ,  $V_2$ , and  $V_3$ , with the masses of 1700 kg, 1400 kg, and 1100 kg, respectively, are applied. The crash pulses of  $V_1$ ,  $V_2$ , and  $V_3$  are shown in Figure 9.

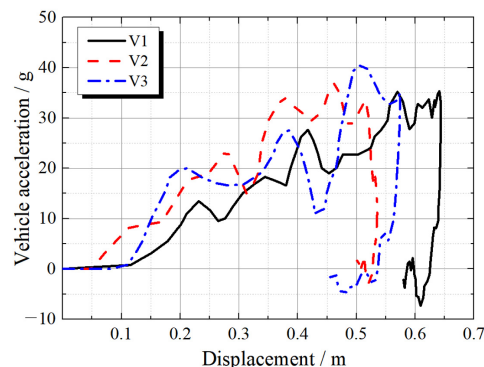


Figure 9. The crash pulses of  $V_1$ ,  $V_2$ , and  $V_3$ .

The stiffness decomposition schemes of the front structures of the three vehicles are all transverse 50% + 25% zone and vertical three floors, denoted as “4 × 3” decomposition, as shown in Figure 10. Decomposition plans ( $Q$ ) of  $V_1$ ,  $V_2$ , and  $V_3$  are obtained as shown in Equation (27).

$$Q(V1) = \begin{bmatrix} 0.080 & 0.070 \\ 0.120 & 0.080 \\ 0.085 & 0.070 \end{bmatrix}, Q(V2) = \begin{bmatrix} 0.080 & 0.070 \\ 0.110 & 0.090 \\ 0.080 & 0.070 \end{bmatrix}, Q(V3) = \begin{bmatrix} 0.090 & 0.060 \\ 0.100 & 0.100 \\ 0.090 & 0.060 \end{bmatrix} \quad (27)$$

$k_{12}$	$k_{11}$	$k_{11}$	$k_{12}$	$Q_{i1}$
$k_{22}$	$k_{21}$	$k_{21}$	$k_{22}$	$Q_{i2}$
$k_{32}$	$k_{31}$	$k_{31}$	$k_{32}$	$Q_{i3}$
$Q_{r1}$	$Q_{r2}$	$Q_{r3}$	$Q_{r4}$	

Figure 10. The decomposition of the crash pulse.

The values of  $OLC$ ,  $MD$ ,  $SD$  and  $PM$  are obtained in Table 1. The errors between the calculation results and the existing data are all about 10%, which indicate that the accuracy of the solution method is acceptable.

Table 1. The values of  $OLC$ ,  $MD$ ,  $SD$ , and  $PM$ .

Vehicles	Results	Evaluation Indexes			
		$OLC$ (g)	$MD$ (m)	$SD$ (mm)	$PM$
V1	Existing data	35.9	Bottoming, $MD > 0.63$	56	3.74
	Calculation	31.30	0.71	63.34	3.38
	Error	−12.26%	Accord	13.1%	−9.6%
V2	Existing data	27.8	NO, $MD < 0.63$	93.5	1.57
	Calculation	27.33	0.62	98.3	1.58
	Error	−1.7%	Accord	5.1%	0.5%
V3	Existing data	26.3	NO, $MD < 0.63$	96.4	1.26
	Calculation	23.75	0.57	107.05	1.14
	Error	−9.7%	Accord	11.04%	−9.5%

### 3.3.3. Verification of Small Overlap Condition

The finite element calculation results of a vehicle in small overlap condition as the basic data are used to verify the accuracy of the analytical model by the maximum intrusion amount of the upper part of the passenger compartment. The vehicle mass is 1365 kg, and the energy absorption space in the front compartment is 0.68 m. The maximum intrusion value of the four intrusion measurement points on the upper part of the passenger compartment is taken as 34.2 cm in the simulation results of the vehicle as shown in Figure 11 [32].

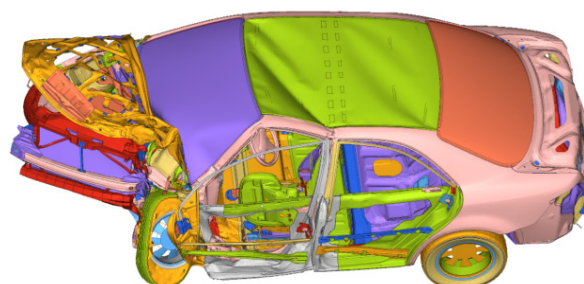


Figure 11. The finite element calculation results of vehicle in FRB.

It is known that the energy absorption decomposition scheme of the front-end structure of the car body is shown in Equation (28). Take the crash pulse of the vehicle as shown in Figure 12 into the analytical model together with the decomposition scheme in Equation (28) to calculate the maximum longitudinal displacement of the vehicle as 1.0019 m. The maximum intrusion value of the passenger compartment calculated by the analytical model is  $1.0019 - 0.68 = 0.3219$  m, and the error with the maximum value of the upper intrusion of the passenger compartment of the finite element model is  $-5.88\%$ . It shows that the analytical model solved in small overlap condition is effective.

$$Q(\text{vehicle}) = \begin{bmatrix} 0.06 & 0.04 \\ 0.21 & 0.10 \\ 0.06 & 0.03 \end{bmatrix} \quad (28)$$

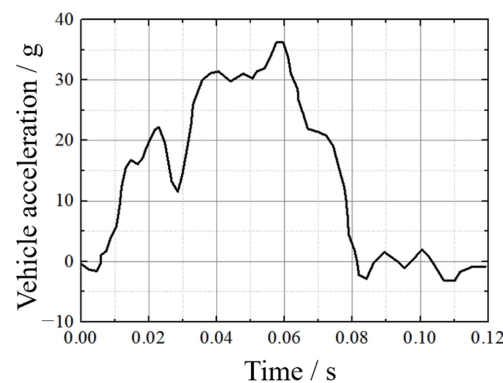


Figure 12. The crash pulse of vehicle in FRB condition.

#### 4. Analysis and Discussion

##### 4.1. Impact Analysis of Different Waveform Decomposition Schemes

In this section, the effect of waveform decomposition scheme on three evaluation indexes of compatibility, i.e., *OLC*, *MD*, and *SD*, is studied. Note that the  $4 \times 3$  decomposition method is adopted in this research. Considering the lateral symmetry of the car body, the variables of the decomposition method are the proportion of energy absorbed by six variables, and the sum of the six variables is 50%, as shown in Equation (28).

$$Q = \begin{bmatrix} q_{11} & q_{12} \\ q_{21} & q_{22} \\ q_{31} & q_{32} \end{bmatrix}, q_{11} + q_{12} + q_{21} + q_{22} + q_{31} + q_{32} = 50\% \quad (29)$$

Three variation schemes for six variables are proposed, as follows:

Alternative 1: setting any one of the six variables to increase from 0 to 50%, and the other variables are equal.

Alternative 2: setting any two of the six variables are increased from 0 to 50%, and the other variables are equal.

Alternative 3: setting any three of the six variables and increase them from 0 to 50%, and the other variables are equal.

The decomposition difference of each scheme is calculated by Equation (29). In addition, the design and decomposition difference (*W*) of the three alternatives are shown in Table 2.

$$W = |q_{11} - q_{12}| + |q_{11} - q_{21}| + |q_{11} - q_{22}| + |q_{11} - q_{31}| + |q_{11} - q_{32}| + |q_{12} - q_{21}| + |q_{12} - q_{22}| + |q_{12} - q_{31}| + |q_{12} - q_{32}| + |q_{21} - q_{22}| + |q_{21} - q_{31}| + |q_{21} - q_{32}| + |q_{22} - q_{31}| + |q_{22} - q_{32}| + |q_{31} - q_{32}| \quad (30)$$

**Table 2.** The design and decomposition difference of the three alternatives.

No.	Alternative A			Alternative B			Alternative C		
	One of $q_{ij}$	Other $q_{ij}$	$W$	Two of $q_{ij}$	Other $q_{ij}$	$W$	Three of $q_{ij}$	Other $q_{ij}$	$W$
1	0	0.10	0.50	0	0.125	1.00	0	0.1667	1.5
2	0.05	0.09	0.20	0.05	0.10	0.40	0.05	0.1177	0.6
3	1/12	0.0833	0	1/12	0.0833	0.00	1/12	0.0833	0
4	0.1	0.08	0.10	0.1	0.075	0.20	0.1	0.0667	0.3
5	0.15	0.07	0.40	0.15	0.05	0.80	0.15	0.0167	1.2
6	0.2	0.06	0.70	0.2	0.025	1.40			
7	0.25	0.05	1	0.25	0	2.00			
8	0.3	0.04	1.30						
9	0.35	0.03	1.60						
10	0.4	0.02	1.90						
11	0.45	0.01	2.20						
12	0.5	0	2.50						

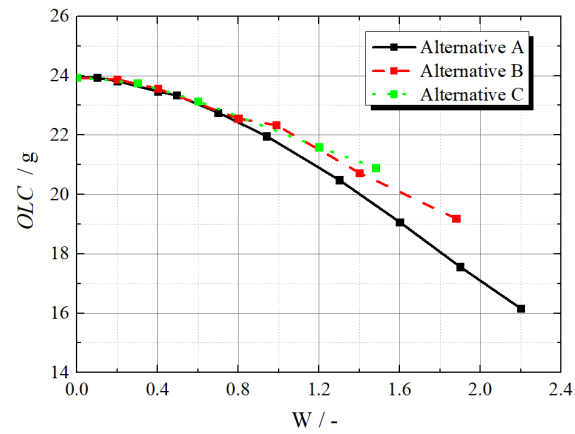
In this section, the decomposition difference and the stiffness-change position of the three schemes are adopted as the criteria to measure the uniformity of the barrier. The greater  $W$  is, the poorer the uniformity of the decomposition scheme. At the same  $W$ , with the more varied locations, the uniformity of the decomposition scheme is better. With  $W$  as the horizontal coordinate, the values of  $OLC$ ,  $MD$ , and  $SD$  calculated by the three schemes are drawn, as shown in Figure 13, respectively.

When  $W$  is 0, the local stiffnesses of vehicle are evenly distributed. As the  $W$  increases, the uniformity becomes worse. Through the above analysis and the information in Figure 13, it is found that when  $W$  is 0, the  $OLC$  is the largest, the  $MD$  is the smallest, and the  $SD$  equals 0. In the Figure 13, as the  $W$  increases, the decomposition scheme becomes more and more uneven, the  $OLC$  value gradually decreases, and the  $MD$  and  $SD$  value gradually increases. Corresponding to the same value of  $W$ , the positional relationship of local stiffness changes in the three stiffness decomposition schemes is: Alternative 3 > Alternative 2 > Alternative 1.

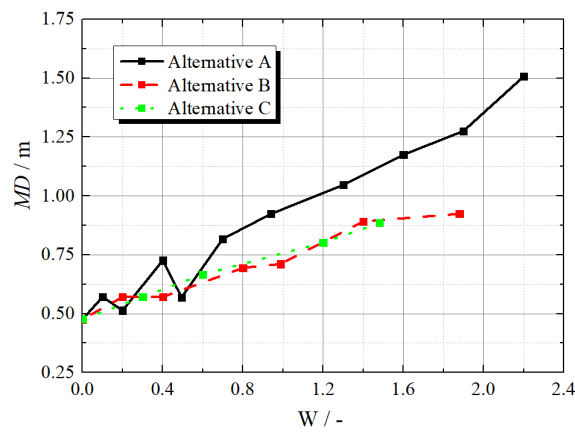
When  $W$  is the same, the  $OLC$  values of three alternatives are basically the same, which shows that  $OLC$  is more sensitive to  $W$ , but has nothing to do with the position of the stiffness distribution. When the  $W$  is the same, the increase in the stiffness-change position helps to reduce the  $MD$ , and increase  $SD$ . It shows that  $MD$  and  $SD$  are more sensitive to the change position of local stiffness and  $W$ . In general, the worse the uniformity of the vehicle stiffness distribution, the smaller the  $OLC$ , and the larger the  $MD$  and  $SD$ . In order to ensure that the barrier is not penetrated and to control the deformation uniformity index  $SD$ , it is necessary to reasonably allocate the stiffness of the front-end structure.

#### 4.2. Discussion about Stiffness Decomposition of Vehicle

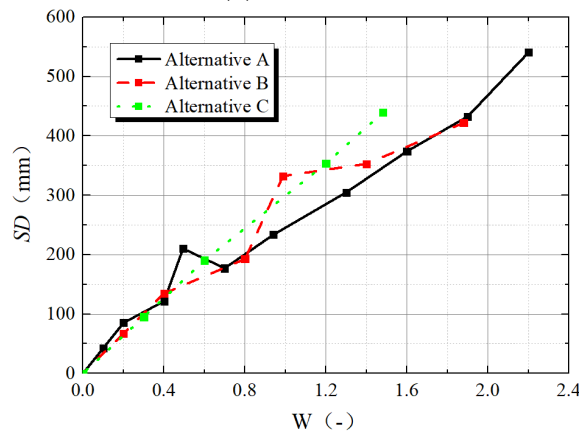
The study of automobile crash safety is very important to improve road traffic safety [33–35]. In the reference [24], an analytical model integrating barrier, vehicle, and occupant is established to obtain not only the system dynamic responses but also the two evaluation indexes in MPDB ( $OLC$  and  $MD$ ), known as BVO model, as shown in Figure 14. The BVO model system refers to simplified models with the elements of masses and springs. It is assumed that vehicle and barrier have constant masses during the impact process. The spring stiffnesses are used to represent the deformation energy absorption process of the structures. Since the overlap between vehicle and barrier are ignored in the modeling, the rotation responses of the BVO system and the local deformation index of barrier  $SD$  cannot be calculated [31,36].



(a) W VS. OLC.



(b) W VS. MD



(c) W VS. SD

Figure 13. The relationships between  $W$  and three compatibility evaluation indexes.

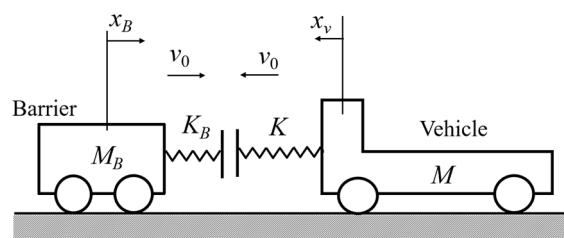


Figure 14. The BVO model.

In order to solve the dynamic response of the vehicle in the overlap impact conditions, the equivalent stiffness of the BVO model ( $K_B$  and  $K$ ) are decomposed into the local stiffness in this paper, as shown in Figure 5. The three-dimensional analytical model of vehicle front end structure after stiffness decomposition is shown in Figure 4. The previous impact mechanics model can solve the one-dimensional dynamic response. The analytical model and solution method proposed in this paper provide new calculation ideas for the three-dimensional dynamic response of the impact system.

The vehicle data as the verification of the analytical model solved in MPDB test, are the same with data to verify the accuracy of BVO model in the reference [24]. The results of the BVO model are calculated by the vehicle mass and the crash pulse in the Section 3.3.2, as shown in Table 3.

**Table 3.** The results of the BVO model.

	Large Vehicle	Medium Vehicle	Small Vehicle
$a_{vmax}$ (g)	30.77	36.14	43.34
$OLC$ (g)	33.15	29.17	25.84
$MD$ (m)	0.63	0.55	0.48

Comparing with the results calculated by the BVO model in Table 3, the  $OLC$  values calculated by the analytical model are smaller and the  $MD$  values are larger. This may be because that the local stiffnesses obtained after decomposing the vehicle stiffness are connected in parallel when the vehicle parameters are the same. The local stiffnesses of vehicle and barrier are first connected in series and then in parallel as the overall equivalent stiffness between the two to calculate the impact responses under the MPDB condition. Therefore, if the decomposition is uniform, the equivalent stiffness between barrier and vehicle is constant, that is, the  $OLC$  and accelerations of the system calculated by the BVO model and proposed analytical model are the same, and the deformation standard deviation  $SD$  of the barrier is 0. If it is not uniformly decomposed, the equivalent stiffness between vehicle and barrier is decreased, so that the  $OLC$  is decreased; and a part of local stiffnesses of vehicle are increased to cause the local deformation of the barrier to increase, i.e.,  $MD$  is increased; at the same time, the  $SD$  value is larger than 0.

In engineering application, the main methods to improve vehicle compatibility are the following: reducing the quality of the entire vehicle, evenly distributing structural stiffness, and designing a reasonable crash pulse [12,13]. In the process of safety development, the quality level of the vehicle should be determined first, then the BVO model should be used to optimize the crash pulse, and finally the proposed model in this paper should be used to decompose the stiffness of front-end structure [7,37].

The effect of vehicle stiffness decomposition on the dynamic responses of small offset impact conditions is not analyzed in this paper. Theoretically, the greater the stiffness of the 25% area (QY1 or QY4 in the Figure 10), the smaller the deformation of the vehicle front-end structure and the smaller intrusion into the passenger compartment. Therefore, in the engineering design, the sum of the stiffness of the three positions in the 25% area should be increased as much as possible to improve the safety of the passenger compartment. That is to say, adding an energy-absorbing structure or increasing the stiffnesses of the existing structures in the 25% area can effectively improve the safety of the vehicle in small offset impact condition.

#### 4.3. Comparison with Existing Research

The energy management method distributes the total collision energy to the various energy absorption structures of the auto body. According to the difference of the decomposition method in time and space order, a variety of energy management methods are proposed. From 2006 to 2011, Qi proposed the magic cube approach which decomposes crashworthiness target into sub-structure design targets, and designs the load of front longitudinal beam by the dynamic topology optimisation method [20,21,38]. In 2011, the book of

'Fundamentals of Automobile Body Structure Design' divided the energy absorption space of the front-end structure according to the transmission path of the impact force [22]. From 2011 to 2013, Zhang et al. effectively decomposed total collision energy into sub-structure performance targets based on energy management technology [25,39]. From 2013 to 2016, Qiu presented an average allocation between ride-down energy and restraint energy to decrease occupant injury; in his book 'Automobile Crash Safety Engineering', the concepts of 'longitudinal energy management' and 'lateral energy management' were proposed [7,40].

The existing researches basically use qualitative methods to decompose the total energy of a frontal vehicular crash into the front-end structures [31,37]. The existing methods rely on empirical data or the subjective judgment of engineers and experts. Compared with the existing methods, the most important feature of this paper is to use an analytical method to optimize the crash energies of the vehicle front-end structures. This analytical method greatly reduces the empirical dependence of the frontal vehicular crash. In addition, the existing studies are based on empirical conclusions of FRB. The multi-conditions crash energy optimization method proposed in this paper is mainly based on the FRB, and takes into account the design requirements of MPDB and SOB.

## 5. Conclusions

This paper studies the modeling method of vehicle front-end structures and the solution method of system dynamic responses in multiple impact conditions to manage the crash energy. The energy absorption space of vehicle front-end is decomposed in three dimensions, and expressed by the spring stiffness to construct the analytical model of the front-end structure. Based on the three-dimensional analytical model of the front-end structure, the dynamic responses and evaluation indexes of the MPDB and SOB operating system are solved by the principle of engineering vibration with input of crash pulse decomposition scheme. Subsequently, the sensitivity of the crash pulse decomposition scheme to the evaluation indicators of each operating condition is analyzed based on the solution method in the multi-condition. Several concluding remarks are drawn as follows:

- (1) comparing the experimental data of the MPDB test and the calculation results of constructed analytical model, the errors of evaluation indexes, i.e., *OLC*, *SD* and *PM*, are all less than 15%, and judgments about the barrier bottoming out are all in accordance;
- (2) comparing the simulation data of the SOB test and the calculation results of constructed analytical model, the errors of the maximum intrusion into passenger compartment is  $-5.88\%$ ;
- (3) as the *W* increases, the decomposition scheme becomes more and more uneven, the *OLC* value gradually decreases, the *MD* and *SD* value gradually increases;
- (4) *OLC* is more sensitive to *W*; *MD* and *SD* are more sensitive to the change position of local stiffness and *W*;
- (5) the greater the stiffness of the 25% area, the smaller the deformation of the vehicle front-end structure and the intrusion into the passenger compartment.

To sum up, the proposed method reveals the energy absorption principle of the front-end structure during the frontal impact process. The calculation results provide references for vehicle crash energy management in three conditions. In the case of insufficient enterprise experience data, the optimization method in this paper can be used to carry out the forward design of frontal vehicular crash safety.

**Supplementary Materials:** The following supporting information can be downloaded at: <https://www.mdpi.com/article/10.3390/su142416913/s1>, Supplementary Information: The main MATLAB algorithm of the solution method is established in the paper.

**Author Contributions:** Conceptualization, D.W. and L.H.; Methodology, J.Z.; Software, S.W.; Writing—original draft, D.W.; Writing—review & editing, L.H. All authors have read and agreed to the published version of the manuscript.

**Funding:** This work was supported by the State Key Laboratory of Automotive Safety and Energy under Project No. KFY2203, and the Natural Science Foundation of Hunan Province (No. 2022JJ40493).

**Institutional Review Board Statement:** Not applicable.

**Informed Consent Statement:** Not applicable.

**Data Availability Statement:** The data used to support the findings of this study are available from the corresponding author upon request.

**Conflicts of Interest:** The authors declare that they have no conflict of interest.

## References

1. Zhang, H.; Peng, Y.; Hou, L.; Tian, G.; Li, Z. A hybrid multi-objective optimization approach for energy-absorbing structures in train collisions. *Inf. Sci.* **2019**, *481*, 491–506. [CrossRef]
2. Zhang, H.; Peng, Y.; Hou, L.; Wang, D.; Tian, G.; Li, Z. Multistage impact energy distribution for whole vehicles in high-speed train collisions: Modeling and solution methodology. *IEEE Trans. Ind. Inform.* **2020**, *16*, 2486–2499. [CrossRef]
3. Bilston, L.; Brown, J.; Whyte, T. Head excursion in frontal impacts is lower in high back booster seats than in forward facing child seats with internal harnesses designed for children up to 8 years of age. *Traffic Inj. Prev.* **2022**, *23*, 244–249. [CrossRef] [PubMed]
4. Reddy, S. Multi-cornered thin-walled sheet metal members for enhanced crashworthiness and occupant protection. *Thin-Walled Struct.* **2015**, *94*, 56–66. [CrossRef]
5. Nguyen, L.P.T. An optimisation approach to choose thickness of three members to improve IIHS small-overlap structural rating. *Int. J. Crashworthiness* **2017**, *22*, 518–526. [CrossRef]
6. Gidlewski, M.; Prochowski, L.; Jemioł, L.; Żardecki, D. The process of front-to-side collision of motor vehicles in terms of energy balance. *Nonlinear Dyn.* **2019**, *97*, 1877–1893. [CrossRef]
7. Qiu, S. *Automobile Crash Safety Engineering*; Institute of Technology Press: Beijing, China, 2016.
8. Huang, M. *Automobile Crash Mechanics*; CRC Press: Boca Raton, FL, USA, 2002.
9. Hu, L.; Zhou, X.; Zhang, X.; Wang, F.; Li, Q.; Wu, W. A review on key challenges in intelligent vehicles: Safety and driver—Oriented features. *IET Intell. Transp. Syst.* **2021**, *15*, 1093–1105. [CrossRef]
10. Othaganont, P.; Assadian, F.; Auger, D.J. Multi-objective optimisation for battery electric vehicle powertrain topologies. *Proc. Inst. Mech. Eng. Part D J. Automob. Eng.* **2017**, *231*, 1046–1065. [CrossRef]
11. Huang, H.; Siddiqui, C.; Abdel-Aty, M. Indexing crash worthiness and crash aggressivity by vehicle type. *Accid. Anal. Prev.* **2011**, *43*, 1364–1370. [CrossRef]
12. Zhang, J. *Parameters Design Method for Structure and Occupant Restraint System in Vehicle Crash*; Science Press: Beijing, China, 2018.
13. Zhang, J.; Wang, D.; Wu, L.; Liu, L. Conceptual design of the front-end structure of automobile considering crashworthiness: A three-stage target decomposition method. *Int. J. Crashworthiness* **2020**, *25*, 183–191. [CrossRef]
14. Mizuno, K. *Crash Safety of Passenger Vehicles*; China Communications Press: Beijing, China, 2016.
15. Teng, T.L.; Chang, P.H.; Liang, C.C. Application of crash pulse on the car crashworthiness design. *Adv. Mech. Eng.* **2017**, *9*, 168781401770009. [CrossRef]
16. Iraeus, J.; Lindquist, M. Analysis of minimum pulse shape information needed for accurate chest injury prediction in real life frontal crashes. *Int. J. Crashworthiness* **2021**, *26*, 684–691. [CrossRef]
17. Tian, G.; Zhang, H.; Feng, Y.; Jia, H.; Zhang, C.; Jiang, Z.; Li, Z.; Li, P. Operation patterns analysis of automotive components remanufacturing industry development in China. *J. Clean. Prod.* **2017**, *164*, 1363–1375. [CrossRef]
18. Shi, Y.; Wu, J.; Nusholtz, G.S. Optimal Frontal Vehicle Crash Pulses—A Numerical Method for Design. In Proceedings of the 18th Enhanced Safety of Vehicles (ESV) Conference, Nagoya, Japan, 19–22 May 2003; p. 514. Available online: [https://www.safetylit.org/citations/index.php?fuseaction=citations.viewdetails&citationIds\[\]=citjournalarticle\\_245671\\_38](https://www.safetylit.org/citations/index.php?fuseaction=citations.viewdetails&citationIds[]=citjournalarticle_245671_38) (accessed on 17 November 2022).
19. Lars, K.; Simon, G.; Konrad, E. Frontal crash pulse assessment with application to occupant safety. *ATZ Worldw.* **2009**, *111*, 12–17.
20. Anselma, P.; Niutta, C.; Mainini, L.; Belingardi, G. Multidisciplinary design optimization for hybrid electric vehicles: Component sizing and multi-fidelity frontal crashworthiness. *Struct. Multidiscip. Optim.* **2020**, *62*, 2149–2166. [CrossRef]
21. Qi, C.; Ma, Z.; Kikuchi, N.; Raju, B. Blast protection design of a military automobile system using a magic cube approach. *SAE SP* **2008**, *2195*, 21.
22. Malen, D. *Fundamentals of Automobile Body Structure Design*; SAE International: Warrendale, PA, USA, 2011.
23. Narukawa, T.; Nishimura, H.; Ito, Y.; Motozawa, Y. Studies on Occupant Restraint Method in Car Crash Using Reduced-Order Dynamic Model Considering Thoracic Deflection. *Nihon Kikai Gakkai Ronbunshu C Hen/Trans. Jpn. Soc. Mech. Eng. Part C* **2013**, *79*, 1396–1405. [CrossRef]
24. Wang, D.; Zhang, J.; Ma, Y.; Jin, Y. Analytical modeling and collaborative optimization of the dynamic responses for barrier-vehicle-occupant system considering crashworthiness and compatibility. *Struct. Multidiscip. Optim.* **2021**, *64*, 349–367. [CrossRef]
25. Zhang, J.; Chen, G.; Liu, L.; Li, H.; Tang, H. Design and target decomposition of impact pulse of car frontal crashworthiness. *J. Jilin Univ. Eng. Technol. Ed.* **2012**, *42*, 823–827.

26. Huang, M.; Laya, J.; Loo, M. A study on ride-down efficiency and occupant responses in high speed crash tests. *SAE Tech. Pap.* **1995**. [[CrossRef](#)]
27. Mizuno, K.; Itakura, T.; Hirabayashi, S.; Tanaka, E.; Ito, D. Optimization of vehicle deceleration to reduce occupant injury risks in frontal impact. *Traffic Inj. Prev.* **2014**, *15*, 48–55. [[CrossRef](#)] [[PubMed](#)]
28. Dima, D.; Covaciu, D. Vehicles Frontal Impact Analysis Using Computer Simulation and Crash Test. *Int. J. Automot. Technol.* **2019**, *20*, 655–661. [[CrossRef](#)]
29. Zou, T.; Shang, S.; Simms, C. Potential benefits of controlled vehicle braking to reduce pedestrian ground contact injuries. *Accid. Anal. Prev.* **2019**, *129*, 94–107. [[CrossRef](#)]
30. Yan, H.; Zhong, L.; Yu, J.; Jiang, W. Research on 2020 E-NCAP MPDB Test. *Automob. Appl. Technol.* **2019**, *21*, 6.
31. Watanabe, T.; Kuroda, I.; Nakajima, T. Relationship between frontal car-to-car test result and vehicle crash compatibility evaluation in mobile progressive deformable barrier test. *Traffic Inj. Prev.* **2019**, *20*, S78–S83. [[CrossRef](#)] [[PubMed](#)]
32. Nguyen, P.; Lee, J.; Yim, H. Analysis of vehicle structural performance during small-overlap frontal impact. *Int. J. Automot. Technol.* **2015**, *16*, 799–805. [[CrossRef](#)]
33. Hu, L.; Tian, Q.; Zou, C.; Huang, J.; Ye, Y.; Wu, X. A study on energy distribution strategy of electric vehicle hybrid energy storage system considering driving style based on real urban driving data. *Renew. Sustain. Energy Rev.* **2022**, *162*, 112416. [[CrossRef](#)]
34. Wang, F.; Yin, J.; Hu, L.; Wang, M.; Liu, M.; Miller, K.; Wittek, A. Should anthropometric differences between the commonly used pedestrian computational biomechanics models and Chinese population be taken into account when predicting pedestrian head kinematics and injury in vehicle collisions in China? *Accid. Anal. Prev.* **2022**, *173*, 106718. [[CrossRef](#)]
35. Farid, A.; Ksaibati, K. Modeling Two-Lane Highway Passing-Related Crashes Using Mixed Ordinal Probit Regression. *J. Transp. Eng. Part A Syst.* **2020**, *9*, 146. [[CrossRef](#)]
36. Tian, G.; Yuan, G.; Aleksandrov, A.; Zhang, T.; Li, Z.; Fathollahi-Fard, A.M.; Ivanov, M. Recycling of spent Lithium-ion Batteries: A comprehensive review for identification of main challenges and future research trends. *Sustain. Energy Technol. Assess.* **2022**, *53*, 102447. [[CrossRef](#)]
37. Wang, K.; Xie, G.; Xiang, J.; Li, T.; Peng, Y.; Wang, J.; Zhang, H. Materials selection of 3D printed polyamide-based composites at different strain rates: A case study of automobile front bumpers. *J. Manuf. Process.* **2022**, *84*, 1449–1462. [[CrossRef](#)]
38. Hu, S.; Ma, Z.D.; Qi, C. Magic Cube approach application on crashworthiness design of front rail in front angle impact. In Proceedings of the 2009 International Conference on Mechatronics and Automation, Changchun, China, 9–12 August 2009; pp. 3521–3526.
39. Zhou, Y.; Lan, F.; Wei, X.A. A Study on the Matching Law of High Strength Steel Sheets for Car-body Front-end Structures Based on Frontal Impact Requirements. *Automot. Eng.* **2009**, *31*, 990–994.
40. Qiu, S.; Li, H.; Zhang, J. Optimized ride-down rate control in frontal impact and its application in the energy management of occupant restraint system. *SAE Tech. Pap.* **2013**. [[CrossRef](#)]